Functionalized Periodic Mesoporous Organosilica Nanoparticles for Loading and Delivery of Suramin

Nikola Ž. Knežević [1,*] , **Sanja Djordjević [2]** , **Vesna Kojić [3]** and **Djordje Janaćković [2]**

[1] BioSense Institute, University of Novi Sad, Dr Zorana Djindjica 1, 21000 Novi Sad, Serbia
[2] Faculty of Technology and Metallurgy, University of Belgrade, Karnegijeva 4, 11000 Belgrade, Serbia; sanjadjordjeviccc@gmail.com (S.D.); nht@tmf.bg.ac.rs (D.J.)
[3] Oncology Institute of Vojvodina, Put Dr Goldmana 4, 21204 Sremska Kamenica, Serbia; vesna.kojic@sbb.rs
[*] Correspondence: nknezevic@biosense.rs or nikola.z.knezevic@gmail.com

Abstract: Suramin (SUR) is a known drug for treating parasitic infections though research studies and some clinical trials have shown its applicability for a plethora of other diseases. Herein we report on a novel SUR nanocarrier for the drug delivery to cells. We synthesized periodic mesoporous organosilica nanoparticles with spherical morphology, having mean diameter of 240 nm and high surface area (778 m^2/g). The material's surface is modified with an amine-containing organic moiety *N*-[3-(Trimethoxysilyl)propyl]ethylenediamine (DA), followed by surface attachment with the drug. The rate of SUR release in physiological condition was low, though in vitro experiments on MRC-5 cell line demonstrate effective delivery of the drug to the cells and low toxicity of the materials without the adsorbed drug. These results are promising for opening new treatment strategies with SUR-bearing nanocarriers, with high efficiency and low adverse effects on healthy tissues.

Keywords: drug delivery; nanocarrier; porous nanoparticles; cancer treatment

1. Introduction

Originally developed for the treatment of parasitic infections such as trypanosomiasis and onchocerciasis, the drug Suramin (SUR) has been known since 1920s. [1]. However, the research studies increasingly reveal new biological targets for SUR, opening up its application for the treatment of different diseases such as AIDS [2], ZIKA virus [3], human enteroviruses [4], and cancer [5,6] while novel small, phase I/II clinical trial even revealed the potential of low doses of SUR for the treatment of Autism [7]. Hence, it is of substantial interest to develop safe SUR nanocarriers for achieving controlled and targeted drug delivery and thus increasing its therapeutic efficacy with inhibiting the occurrence of side effects.

SUR nanocarriers were previously constructed by entrapping the drug within surfactant-silica hybrid nanoparticles in situ, i.e., during the synthesis procedure of the material, and demonstrated for effective anti-angiogenic application [8]. Herein, we investigate the potential of pre-synthesized periodic mesoporous organosilica (PMO) nanomaterial to act as a platform for surface adsorption and delivery of SUR. PMO nanoparticles are distinguished as highly promising for drug delivery and other applications [9–13], predominantly due to their high surface area, possibilities for versatile surface modifications, stimuli-responsive degradability and high biocompatibility. Previously, we demonstrated the potential of PMO nanoparticles for efficient cancer therapy and diagnostics [14,15], as well as for skin protection from UV irradiation [16]. Mesoporus silica nanoparticles (MSN) are more studied structural analogues of PMO for cancer therapy and plethora of other applications [17–21]. MSN and PMO have the same silica surface though the inner composition of PMO particles is composed of organic bridges, while MSN is made entirely of SiO$_2$ framework, which may offer

significant benefits for PMO in terms of biocompatibility, biodegradability, photoluminescence and other novel properties [22]. Herein, we constructed ethylene-bridged PMO nanoparticles (PMOBTE) and functionalized their surface with *N*-[3-(trimethoxysilyl)propyl]-ethylenediamine in order to favor the interaction of the positively charged amine moieties in aqueous environment with the negatively charged sulfonate groups from the SUR molecule and enhance the drug loading. The efficacy of the drug loaded material for delivery of SUR was further investigated by in vitro experiments on human fetal lung fibroblast MRC-5 cell line. This cell line was chosen to demonstrate the proof of concept for drug delivery to cancer cells but also the previous studies evidence that these healthy fibroblast cells promote cancer cell motility and invasiveness [23], which identifies them as a potential target for battling cancer, if the treatment is localized to the tumor microenvironment.

2. Results and Discussion

Scanning electron micrograph (SEM) image of PMOBTE is shown on Figure 1a. The material consists of spherical nanoparticles with diameters in the range 110–380 nm, though the most nanoparticles are of the size 240 ± 30 nm. Nitrogen sorption analysis revealed that the material possesses high Brunauer–Emmett–Teller (BET) surface area (778 m^2/g) with Barrett–Joyner–Halenda (BJH) pore determination indicating microporous nature of the nanoparticles (<2 nm) with a shoulder in the mesoporous region (2.8 nm). The material has a wormhole porous structure, as evidenced by the transmission electron micrograph (TEM) image (inset on Figure 1a).
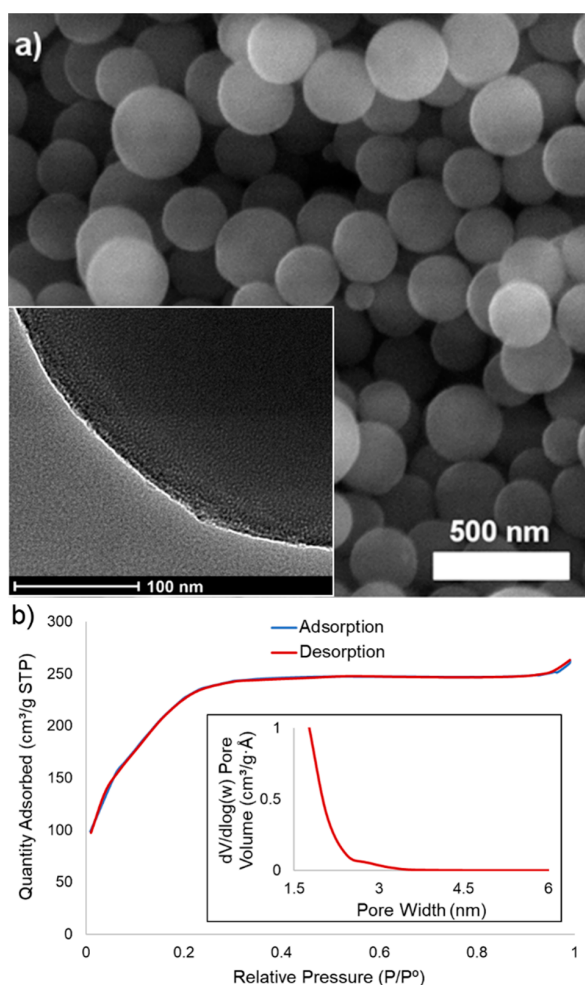

Figure 1. Characterization of ethylene-bridged PMO nanoparticles (PMOBTE) material with: (**a**) scanning electron micrograph and transmission electron micrograph (inset) (**b**) nitrogen adsorption–desorption isotherm and Barrett–Joyner–Halenda (BJH) pore size distribution plot (inset).

The material was functionalized with *N*-[3-(trimethoxysilyl)propyl]ethylenediamine (DA) followed by adsorption of SUR on its surface. Functionalized material was loaded with the drug SUR through electrostatic interaction between the positively charged amine groups on the PMO surface and the negatively charged sufonate groups of SUR. The amount of adsorbed SUR was determined by comparison of starting and the final concentration of the drug during the loading procedure. This calculated amount was 83 µg of SUR per milligram of PMOBTE or 8.3 wt %. The infrared spectroscopy (Figure 2a) confirmed the structure of PMOBTE, the presence of surface functionalized DA and successful loading of SUR. All the spectra contain the peaks at 1412 cm^{-1} (CH_2 δ) and at 1272 cm^{-1} (CH_2–Si δ) vibrations of the bridging ethylene moiety within the framework. In the range 1000–1200 cm^{-1} all the spectra show peaks from different Si–O vibrations within the nanoparticles or on its surface. Upon surface functionalization with DA, the appearance of strong band centered at 1655 cm^{-1} is evident, which is characteristic for δ NH_2 and NH vibrations from the functionalized moiety. The broader peak of weaker intensity at 1631 cm^{-1} in the spectrum of PMOBTE is typical for the surface-adsorbed water. In the spectrum of the SUR (Figure 2b)-adsorbed material (SUR@DA-PMOBTE) SUR S=O valence vibration is evident as an additional peak in the heavily overlapping area 1000–1200 cm^{-1}, centered at 1136 cm^{-1} while the appearance of amide band of SUR is also noticeable in the spectrum of SUR@DA-PMOBTE, centered at 1542 cm^{-1}.
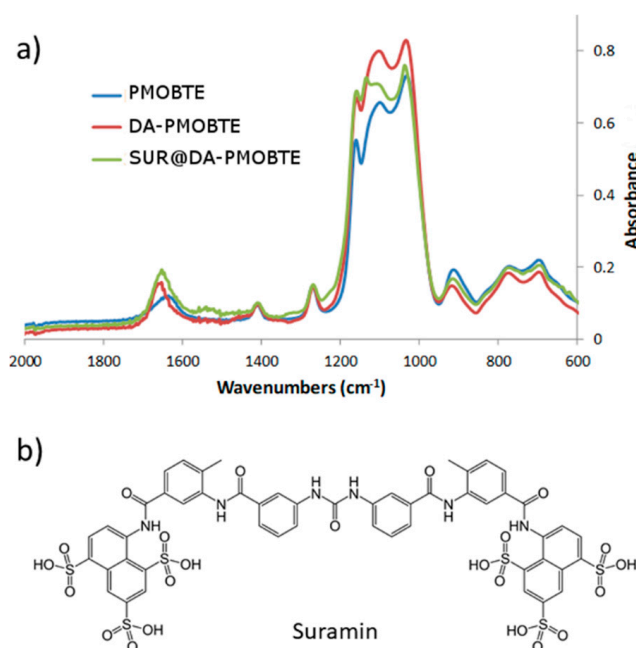

Figure 2. (**a**) Infrared spectra of the synthesized materials and (**b**) the molecular structure of Suramin (SUR).

The structure of the synthesized materials was further confirmed by thermogravimetric (TGA) analyses (Figure 3). All three materials show significant weight loss below 100 °C due to surface-adsorbed water. The material PMOBTE shows a single sharp loss of mass centered at 462 °C, which can be ascribed to the bridging ethylene group. In case of DA-PMOBTE, more complex weight loss pattern is observed, clearly evidencing successful functionalization of PMOBTE. The weight loss centered at 176 °C can be attributed to chemically bonded water molecules to the surface, i.e., possibly hydroxyl ions, attached to the amine groups of the functionalized DA moiety. The difference in weight loss above 250 °C between DA-PMOBTE and PMOBTE indicates the amount of grafted DA on the surface (14.7 wt %). Significant loss of weight for both DA-PMOBTE and SUR@DA-PMO is observed above 300 °C, with two major bands, observed in the Derivative weight plot, centered at 361 and 540 °C for DA-PMOBTE and at 358 and 530 °C for SUR@DA-PMOBTE. The shift of these bands as well as the change in their relative intensity indicates the successful attachment of SUR to the

surface. Furthermore, in case of SUR@DA-PMOBTE the weight loss at 176 °C is less pronounced when compared to the analysis of DA-PMOBTE, as SUR replaced the hydroxyl groups as the counterion for amine groups of the functionalized DA, while a new weak band in the Derivative weight plot appears at 300 °C.
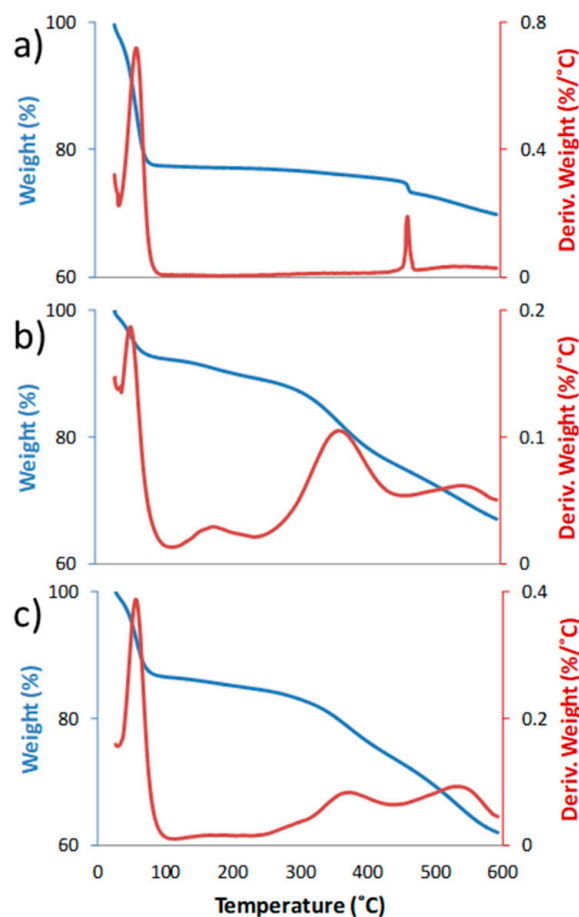

Figure 3. Thermogravimetric analysis (TGA) of PMOBTE (**a**), *N*-[3-(Trimethoxysilyl)propyl] ethylenediamine (DA)-PMOBTE (**b**) and SUR@DA-PMOBTE (**c**).

The drug release was measured from a stirred suspension (1 mg/mL) in PBS buffer (pH 7.4). As can be seen from Figure 4a the release of the drug from the surface was rather slow, which continued at a constant rate for the duration of the experiment (7 days). In these experimental conditions, with the concentration of material in suspension 1 mg/mL, the average rate of drug release from the material is 1.9 μg of SUR per day, per mg of SUR@DA-PMOBTE. The total release amount of SUR after 7 days was 17% of the total amount loaded on the material. The slow drug release also suggests that the drug is adsorbed on the entire surface of the material (both on external surface and on the surface inside the pores). In case of drug adsorption on the external surface the release is typically fast as all adsorbed molecules are easily available for the exchange with the bulk water molecules and PBS ions. In case of the drug adsorbed inside the mesopores, the slow diffusion rate of water going inside and of the drug going outside of the pores significantly lowers the rate of drug release, particularly in case of the material like PMOBTE, which has mostly narrow micropores of irregular, wormlike structure. Previous reports demonstrated that decreasing the pore size lowers the rate of drug release for mesoporous silica nanomaterials [24,25].
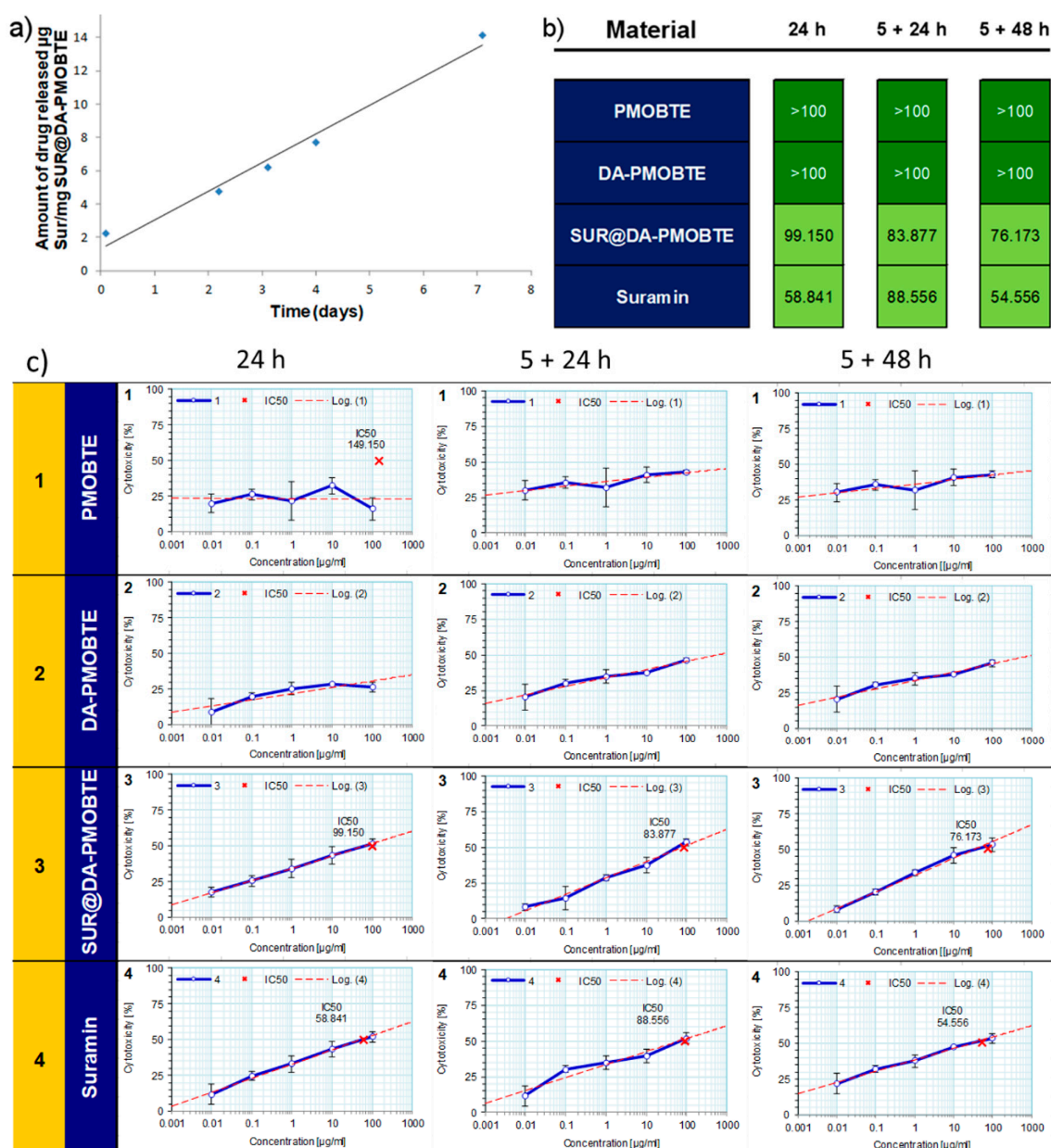
Figure 4. (**a**) Release kinetics of SUR from SUR@DA-PMOBTE in PBS buffer; (**b**) the half maximal inhibitory concentration (IC_{50}) values (expressed in μg/mL) for the MRC-5 cells treated with the synthesized materials and solution of SUR. The suspension of the materials or drug solution were in contact with the cells for 24 h, or for 5 h, followed by 24 h or 48 h of growth in the fresh medium, as indicated; (**c**) Cytotoxicity results for the treatment of MRC-5 cells with prepared materials.

Cell viability experiment on MRC-5 cells (Figure 4b) demonstrated that both materials without SUR (PMOBTE and DA-PMOBTE) showed high biocompatibility with the half maximal inhibitory concentration (IC_{50}) values above 100 μg/mL. SUR loaded materials SUR@DA-PMOBTE showed increased capability to cause cell death and shows IC_{50} values comparable the free SUR, even though the portion of SUR in SUR@DA-PMOBTE material is only 8.3 wt %. This result showcases that DA-PMOBTE as a drug carrier increases the uptake of SUR by the cells and thus increases the treatment efficacy by the loaded drug. Hence, using DA-PMOBTE as a drug carrier would lower amounts of the drug necessary for the therapeutic activity and hence would lower the probability for adverse effects on healthy tissues.

3. Materials and Methods

3.1. Methodology

Scanning electron microscopy (SEM) images were obtained on the Tescan MIRA3 XMU FESEM (Tescan, Brno, Czech Republic), with the electron energies of 20 kV in a high vacuum. The samples were coated with thin layer of Au using a standard sputtering technique. Nitrogen adsorption desorption measurements were conducted on ASAP 2020 (Micromeritics, Norcross, GA, USA) instrument after degassing samples for 6 hours at 105 °C. The TG/DTA analyses were performed simultaneously (30–800 °C range) on an SDT Q600 TGA/DSC instrument (TA Instruments, New Castle, DE, USA). The heating rates were 20 °C/min using less than 10 mg sample mass. The furnace atmosphere consisted of air at a flow rate of 100 cm^3/min. UV/VIS absorbance spectra were recorded on Shimadzu 1800 UV/Vis spectrophotometer (Shimadzu, Kyoto, Japan). FTIR spectra have been obtained by the transmission KBr pellet technique using Thermo-Nicolet Nexus 670 instrument (Thermo Fisher Scientific, Waltham, MA, USA). All reagents were purchased (Sigma-Aldrich, St. Louis, MO, USA) and used as received.

3.2. Synthesis of PMOBTE Nanomaterial

Cetyltrimethylammonium bromide (CTAB, 320 mg) was dissolved in a mixture of ethanol (25.6 mL) and water (28.8 mL). Solution of ammonium hydroxyde (25%, 0.4 mL) was added and the mixture was magnetically stirred at room temperature. The organosilica reagent (1,2-bis(triethoxysilyl)ethane, 0.578 mL) was then added dropwise and the reaction mixture continuously stirred for 24 h at 700 rpm. After this time acetone was added to coagulate the nanoparticles and to facilitate the separation by centifugation. The product was centrifuged at 11,000 rpm, washed twice with water, once with acetone and dried at 80 °C. CTAB was then washed by sonication (twice) in solution of NH_4NO_3 in ethanol (6 g/L) and further washing with ethanol twice and once with acetone.

3.3. Synthesis of DA-PMOBTE Nanomaterial

PMOBTE material (90 mg) was suspended in dry dimethylformamide (DMF, 20 mL), functionalized with *N*-[3-(Trimethoxysilyl)propyl]ethylenediamine (DA, 0.5 mL) by refluxing the mixture at 110 °C over night. The material was then washed twice with water and acetone and dried at 80 °C.

3.4. Synthesis of SUR@DA-PMOBTE Nanomaterial

SUR (SUR, 5.1 mg) was dissolved in 10 mL of ethanol and 1 mL of PBS buffer (pH 7.4) was added. DA-PMOBTE (60 mg) was then added to the solution and stirred for 24 h at room temperature. The material was then isolated by centrifugation at 11,000 rpm and washed twice with ethanol.

The supernatans were collected and evaporated. The residue was dissolved in 20 mL of PBS buffer and the amount of left-over SUR was determined by UV/VIS absorbance at 237 nm, from the previously prepared standard curve. The difference between the starting and residue amounts of SUR gives the amount of loaded SUR, calculated as 83 μg of SUR per mg of SUR@DA-PMOBTE material.

3.5. Drug Release Experiment

For determining the drug release kinetics, the suspension of the SUR@DA-PMOBTE in PBS buffer was prepared (1 mg/mL) and the amount of released SUR was monitored for the period of 7 days. The measurements were conducted on supernatants, after removal of the material by centrifugation at 11,000 rpm from aliquots of the sample solution, by measuring the UV/VIS absorbance at 237 nm and calculating the amount of released drug from the previously prepared standard curve.

3.6. Cell Line Experiments

Experimental procedure was performed using human lung fibroblasts (MRC-5 ATCC CCL 171). Cell lines were cultured in Dulbecco's modified Eagle's medium with 4.5 g/L glucose (DMEM, Sigma-Aldrich, St. Louis, MO, USA), 10% FBS (fetal bovine serum, Sigma) and containing antibiotic/antimycotic solution (Sigma). The cell lines were grown in thermostat at 37 °C with 100% humidity and 5% CO_2 (Heraeus, Hanau, Germany). The cells were passaged twice a week; those used in the experiments were in the logarithmic phase of growth between the third and the tenth passage. The number of cells and their viability were determined using the dye exclusion test with 0.1% trypan blue (DET, data not shown) [26].

3.7. MTT Assay

Growth inhibition was evaluated by tetrazolium colorimetric MTT assay (Sigma-Aldrich, St. Louis, MO, USA). The assay is based on the cleavage of the tetrazolium salt 3-(4,5-dimethylthiazol-2-yl)-2,5-diphenyl tetrazolium bromide (MTT), to formazan by mitochondrial dehydrogenases in viable cells [27]. Exponentially growing cells were harvested, counted by trypan blue and plated into 96-well microtitar plates (Costar) at optimal seeding density of 5×10^3 cells per well to assure logarithmic growth rate throughout the assay period. Viable cells were plated in a volume of 90 μL per well, and preincubated only in DMEM at 37 °C for 24 h to allow cell stabilization prior to the addition of substances. Tested substances dissolved in DMEM medium were added to all wells (10 μL/well) except to the control ones and microplates were incubated for 5 and 24 h. After 5 h the suspensions were removed, the cells were washed with PBS buffer and fresh aliquots of DMEM medium were added and incubated for 24 and 48 h. Three hours before the end of incubation period 10 μL of MTT solution was added to all wells. MTT was dissolved in medium at 5 mg/mL and filtered to sterilize and remove a small amount of insoluble residue present in some batches of MTT. Acid-isopropanol (100 μL of 0.04 N HCl in isopropanol) solution was added to all wells and mixed thoroughly to dissolve the dark blue crystals. After a few minutes at room temperature to ensure that all crystals were dissolved, the plates were read on a spectrophotometer plate reader (Multiscan MCC340, Labsystems Diagnostics Oy, Vantaa, Finland at 540/690 nm. The wells without cells containing complete medium and MTT only acted as blank. Inhibition of growth was expressed as a percent of a control and cytotoxicity was calculated according to the formula: $(1 - OD_{test}/OD_{control}) \times 100$. The substance potency was expressed as the IC_{50} (50% inhibitory concentration).

3.8. Data Analysis

Two independent experiments were set out with quadruplicate wells for each concentration of the compound. IC_{50} value defines the dose of compound that inhibits cell growth by 50%. The IC_{50} of compounds was determined by Median effect analysis.

4. Conclusions

We successfully synthesized periodic mesoporous organosilica nanoparticles with spherical morphology, mean diameter of 240 nm and high surface area (778 m^2/g). The material's surface was functionalized with propyl-ethylenediamine groups and SUR was successfully adsorbed to the surface in the amount of 8.3 wt %. The rate of release of SUR in PBS was low, with only 17% of the loaded drug released after 7 days. However, in vitro experiments on MRC-5 cell line demonstrated high toxicity of the drug loaded material and low toxicity of the materials without the adsorbed drug. These results may open the more efficient treatment possibilities with SUR nanocarriers, with lower adverse effects on healthy tissues.

Conflicts of Interest: The authors declare no conflict of interest.

References

1. Steverding, D. The Development of Drugs for Treatment of Sleeping Sickness: A Historical Review. *Parasit. Vectors* **2010**, *3*, 15. [CrossRef] [PubMed]

2. Rouvroy, D.; Bogaerts, J.; Habyarimana, J.B.; Nzaramba, D.; Van de Perre, P. Short-Term Results with SUR for AIDS-Related Conditions. *Lancet* **1985**, *325*, 878–879. [CrossRef]

3. Albulescu, I.C.; Kovacikova, K.; Tas, A.; Snijder, E.J.; van Hemert, M.J. SUR Inhibits Zika Virus Replication by Interfering with Virus Attachment and Release of Infectious Particles. *Antivir. Res.* **2017**, *143*, 230–236. [CrossRef]

4. Ren, P.; Zheng, Y.; Wang, W.; Hong, L.; Delpeyroux, F.; Arenzana-Seisdedos, F.; Altmeyer, R. SUR Interacts with the Positively Charged Region Surrounding the 5-Fold Axis of the EV-A71 Capsid and Inhibits Multiple Enterovirus A. *Sci. Rep.* **2017**, *7*, 42902. [CrossRef] [PubMed]

5. Gagliardi, A.; Hadd, H.; Collins, D.C. Inhibition of Angiogenesis by SUR. *Cancer Res.* **1992**, *52*, 5073–5075. [PubMed]

6. Li, H.; Li, H.; Qu, H.; Zhao, M.; Yuan, B.; Cao, M.; Cui, J. SUR Inhibits Cell Proliferation in Ovarian and Cervical Cancer by Downregulating Heparanase Expression. *Cancer Cell Int.* **2015**, *15*, 52. [CrossRef] [PubMed]

7. Naviaux, R.K.; Curtis, B.; Li, K.; Naviaux, J.C.; Bright, A.T.; Reiner, G.E.; Westerfield, M.; Goh, S.; Alaynick, W.A.; Wang, L.; et al. Low-Dose SUR in Autism Spectrum Disorder: A Small, Phase I/II, Randomized Clinical Trial. *Ann. Clin. Transl. Neurol.* **2017**, *4*, 491–505. [CrossRef]

8. Veeranarayanan, S.; Poulose, A.C.; Sheikh Mohamed, M.; Nagaoka, Y.; Kashiwada, S.; Maekawa, T.; Sakthi Kumar, D. FITC/SUR Harboring Silica Nanoformulations for Cellular and Embryonic Imaging/Anti-Angiogenic Theranostics. *J. Mater. Chem. B* **2015**, *3*, 8079–8087. [CrossRef]

9. Van Der Voort, P.; Esquivel, D.; De Canck, E.; Goethals, F.; Van Driessche, I.; Romero-Salguero, F.J. Periodic Mesoporous Organosilicas: From Simple to Complex Bridges; a Comprehensive Overview of Functions, Morphologies and Applications. *Chem. Soc. Rev.* **2013**, *42*, 3913–3955. [CrossRef]

10. Croissant, J.G.; Cattoën, X.; Wong Chi Man, M.; Durand, J.-O.; Khashab, N.M. Syntheses and Applications of Periodic Mesoporous Organosilica Nanoparticles. *Nanoscale* **2015**, *7*, 20318–20334. [CrossRef]

11. Croissant, J.G.; Fatieiev, Y.; Omar, H.; Anjum, D.H.; Gurinov, A.; Lu, J.; Tamanoi, F.; Zink, J.I.; Khashab, N.M. Periodic Mesoporous Organosilica Nanoparticles with Controlled Morphologies and High Drug/Dye Loadings for Multicargo Delivery in Cancer Cells. *Chem. A Eur. J.* **2016**, *22*, 9607–9615. [CrossRef]

12. Borah, P.; Sreejith, S.; Anees, P.; Menon, N.V.; Kang, Y.; Ajayaghosh, A.; Zhao, Y. Near-IR Squaraine Dye–loaded Gated Periodic Mesoporous Organosilica for Photo-Oxidation of Phenol in a Continuous-Flow Device. *Sci. Adv.* **2015**, *1*, e1500390. [CrossRef] [PubMed]

13. Wu, L.; Yang, Y.; Ye, Y.; Yu, Z.; Song, Z.; Chen, S.; Chen, L.; Zhang, Z.; Xiang, S. Loading Acid–Base Pairs into Periodic Mesoporous Organosilica for High Anhydrous Proton Conductivity over a Wide Operating Temperature Window. *ACS Appl. Energy Mater.* **2018**, *1*, 5068–5074. [CrossRef]

14. Jimenez, C.M.; Knezevic, N.Z.; Rubio, Y.G.; Szunerits, S.; Boukherroub, R.; Teodorescu, F.; Croissant, J.G.; Hocine, O.; Seric, M.; Raehm, L.; et al. Nanodiamond-PMO for Two-Photon PDT and Drug Delivery. *J. Mater. Chem. B* **2016**, *4*, 5803–5808. [CrossRef]

15. Knežević, N.; Kaluđerović, G.N. Silicon-Based Nanotheranostics. *Nanoscale* **2017**, *9*, 12821–12829. [CrossRef]

16. Knežević, N.Ž.; Ilić, N.; Dokić, V.; Petrović, R.; Janaćković, D. Mesoporous Silica and Organosilica Nanomaterials as UV-Blocking Agents. *ACS Appl. Mater. Interfaces* **2018**, *10*, 20231–20236. [CrossRef] [PubMed]

17. Knežević, N.Ž.; Gadjanski, I.; Durand, J.-O. Magnetic Nanoarchitectures for Cancer Sensing, Imaging and Therapy. *J. Mater. Chem. B* **2019**, *7*, 9–23. [CrossRef]

18. Knežević, N.Z. Visible Light Responsive Anticancer Treatment with an Amsacrine-Loaded Mesoporous Silica-Based Nanodevice. *RSC Adv.* **2013**, *3*, 19388–19392. [CrossRef]

19.   Huang, P.-K.; Lin, S.-X.; Tsai, M.-J.; Leong, K.M.; Lin, S.-R.; Kankala, K.R.; Lee, C.-H.; Weng, C.-F. Encapsulation of 16-Hydroxycleroda-3,13-Dine-16,15-Olide in Mesoporous Silica Nanoparticles as a Natural Dipeptidyl Peptidase-4 Inhibitor Potentiated Hypoglycemia in Diabetic Mice. *Nanomaterials* **2017**, *7*, 112. [CrossRef] [PubMed]

20.   Kankala, R.K.; Liu, C.-G.; Chen, A.-Z.; Wang, S.-B.; Xu, P.-Y.; Mende, L.K.; Liu, C.-L.; Lee, C.-H.; Hu, Y.-F. Overcoming Multidrug Resistance through the Synergistic Effects of Hierarchical PH-Sensitive, ROS-Generating Nanoreactors. *ACS Biomater. Sci. Eng.* **2017**, *3*, 2431–2442. [CrossRef]

21.   Kankala, R.K.; Kuthati, Y.; Liu, C.-L.; Mou, C.-Y.; Lee, C.-H. Killing Cancer Cells by Delivering a Nanoreactor for Inhibition of Catalase and Catalytically Enhancing Intracellular Levels of ROS. *RSC Adv.* **2015**, *5*, 86072–86081. [CrossRef]

22.   Croissant, J.G.; Fatieiev, Y.; Almalik, A.; Khashab, N.M. Mesoporous Silica and Organosilica Nanoparticles: Physical Chemistry, Biosafety, Delivery Strategies, and Biomedical Applications. *Adv. Healthc. Mater.* **2018**, *7*, 1700831. [CrossRef] [PubMed]

23.   Ding, S.; Chen, G.; Zhang, W.; Xing, C.; Xu, X.; Xie, H.; Lu, A.; Chen, K.; Guo, H.; Ren, Z.; et al. MRC-5 Fibroblast-Conditioned Medium Influences Multiple Pathways Regulating Invasion, Migration, Proliferation, and Apoptosis in Hepatocellular Carcinoma. *J. Transl. Med.* **2015**, *13*, 237. [CrossRef] [PubMed]

24.   Gao, Y.; Chen, Y.; Ji, X.; He, X.; Yin, Q.; Zhang, Z.; Shi, J.; Li, Y. Controlled Intracellular Release of Doxorubicin in Multidrug-Resistant Cancer Cells by Tuning the Shell-Pore Sizes of Mesoporous Silica Nanoparticles. *ACS Nano* **2011**, *5*, 9788–9798. [CrossRef] [PubMed]

25.   Jia, L.; Shen, J.; Li, Z.; Zhang, D.; Zhang, Q.; Duan, C.; Liu, G.; Zheng, D.; Liu, Y.; Tian, X. Successfully Tailoring the Pore Size of Mesoporous Silica Nanoparticles: Exploitation of Delivery Systems for Poorly Water-Soluble Drugs. *Int. J. Pharm.* **2012**, *439*, 81–91. [CrossRef] [PubMed]

26.   Phillips, H.J. CHAPTER 3—Dye Exclusion Tests for Cell Viability. In *Tissue Culture: Methods and Applications*; Kruse, P.F., Patterson, M.K., Eds.; Academic Press: New York, NY, USA, 1973; pp. 406–408.

27.   Mosmann, T. Rapid Colorimetric Assay for Cellular Growth and Survival: Application to Proliferation and Cytotoxicity Assays. *J. Immunol. Methods* **1983**, *65*, 55–63. [CrossRef]